

Semi-empirical model to determine pre- and post-neutron fission product yields and neutron multiplicity

Jounghwa LEE and Young-Ouk LEE

*Nuclear Physics Application Research Division,
Korea Atomic Energy Research Institute, Daejeon 34057, Korea*

Tae-Sun PARK

Center for Exotic Nuclei Studies, Institute for Basic Science, Daejeon 34126, Korea

Peter SCHILLEBEECKX

*European Commission Joint Research Centre,
Directorate G, Retieseweg 111, 2440 Geel, Belgium*

Seung-Woo HONG*

Department of Physics, Sungkyunkwan University, Suwon 16419, Korea

(Received 6 January 2021)

Abstract

Post-neutron emission fission product mass distributions are calculated by using pre-neutron emission fission product yields (FPYs) and neutron multiplicity. A semi-empirical model is used to calculate the pre-neutron FPY, first. Then the neutron multiplicity for each fission fragment mass is used to convert the pre-neutron FPY to the post-neutron FPY. In doing so, assumptions are made for the probability for a pre-emission fission fragment with a mass number A^* to decay to a post-emission fragment with a mass number A . The resulting post-neutron FPYs are compared with the data available. The systems where the experimental data of not only the pre- and post-neutron FPY but also neutron multiplicity are available are the thermal neutron-induced fission of ^{233}U , ^{235}U and ^{239}Pu . Thus, we applied the model calculations to these systems and compared the calculation results with those from the GEF and the data from the ENDF and the EXFOR libraries. Both the pre- and post-neutron fission product mass distributions calculated by using the semi-empirical model and the neutron multiplicity reproduce the overall features of the experimental data.

Keywords: Fission product yield, Neutron multiplicity, Poisson distribution

*E-mail: swhong@skku.ac.kr

I. INTRODUCTION

Fission observables such as fission product yields (FPYs), neutron multiplicity, and kinetic energy distributions are important quantities to understand the dynamics of fission. In particular, the fission fragment mass distribution is one of the most frequently measured observables. Right after scission, fission fragments are highly neutron-rich and de-excite through the emission of neutron and gamma rays. The fission products before and after the emission of neutrons, referred to as *pre*-neutron and *post*-neutron emission fission fragments, respectively, can be related through the emitted neutrons, i.e., neutron multiplicity if we consider only binary fission. To have a comprehensive understanding of the fission process, one needs to describe consistently both pre- and post-neutron FPY data by taking into account the neutron multiplicity. For post-neutron emission FPY (POST-FPY), many data are accumulated, and evaluated fission yield data are available for a wide range of fission systems in the evaluated libraries such as the ENDF [1] and the JEFF [2], but there are only a few experiments in which the pre-neutron emission FPY (PRE-FPY) is measured (indirectly). Theoretically, many studies of fission fragments including microscopic approaches [3–6] and stochastic approaches [7–11] were made to calculate the PRE-FPY through the evolution of a compound nucleus whereas the POST-FPY was rarely investigated, which is important in the applications such as the calculation of decay heat or prediction of fission fragment inventory. Recently, there was a study [12] where the POST-FPY was calculated from the PRE-FPY by using the Hauser-Feshbach model. The Hauser-Feshbach model can treat the statistical decay of nuclei by particle emission, but still relies on empirical models for initial conditions such as spin and parity distribution and excitation energy distribution, which are essential for computation but not well known. On the other hand, if data are available for the neutron multiplicities, a data-driven model can be useful in calculating the POST-FPY based on the multiplicity data. For such a purpose, we attempt to calculate the POST-FPY from the PRE-FPY by using neutron multiplicity data.

A simple semi-empirical model was proposed recently for the calculation of the POST-FPY of uranium [13] and plutonium [14] isotopes by taking into account the emission of prompt neutrons through the *average* number of neutrons emitted for each *compound* nucleus, whereas the number of emitted neutrons depends on each individual fission fragment. Therefore, in this work we attempt to calculate both PRE- and POST-FPYs with

our semi-empirical fission model by taking into account the number of emitted neutrons for each individual fission fragment mass. We show that both the PRE- and POST-FPYs can be reproduced consistently by using the neutron multiplicity data. For that, the number of neutrons emitted from *each* fission fragment mass is needed. We thus consider only the cases of thermal neutron-induced fission of ^{233}U , ^{235}U and ^{239}Pu , where the experimental data are available for both PRE- and POST-FPYs as well as the neutron multiplicity for each fission fragment mass. We first apply the semi-empirical FPY model to the *pre*-neutron emission fission fragment mass distributions instead of the POST-FPY data as was done in Refs. [13, 14]. Then, the post-neutron fission fragment mass distributions can be calculated by taking into account the neutron multiplicity for each fission fragment mass. In doing so, the probability for pre-neutron emission fragments with a mass number A^* to decay to post-neutron emission fragments with a mass number A is needed. We thus make assumptions for the probability in three different ways based on the experimental neutron multiplicity data. The POST-FPYs calculated by using the assumptions are compared with the POST-FPYs from the experimental data [15–25], the ENDF/B-VII.1 [1], and the GEF [26]. It is shown that the PRE- and POST-FPYs calculated by using the assumptions based on the experimental neutron multiplicity data can reproduce both PRE- and POST-FPY experimental data consistently.

II. MODEL FOR PRE-NEUTRON FPY

Let us begin with a brief description of the model [13]. It is based on the work by Bohr and Wheeler [27], where the compound nucleus formed during the fission process is considered as a microcanonical ensemble. The assumption that the fission yield $Y(N, E^*)$ of fission fragments characterized by the neutron number N is determined by the level density at the fission barrier leads us to [28, 29]

$$Y(N, E^*) = Y_0 \exp\left(2\sqrt{\tilde{a}(E^* - V(N))}\right), \quad (1)$$

where Y_0 is an overall normalization factor, \tilde{a} is the level density parameter, and $E^* = E_n + S(n)$ is the excitation energy of a compound nucleus, deduced from the neutron separation energy $S(n)$ of the compound nucleus and the incident neutron energy E_n . The fission

barrier $V(N)$ in Eq. (1) can be written as

$$V(N) = V_{mac}(N) + V_{sh}(N) \exp(-\gamma\varepsilon(N)) \quad (2)$$

with

$$\begin{aligned} V_{mac}(N) &= C_{mac} \left(N - \frac{N_{CN}}{2} \right)^2 + V_0, \\ V_{sh}(N) &= \\ &C_{in} \left[\exp \left(-\frac{(N - N_{in})^2}{\sigma_{in}^2} \right) + \exp \left(-\frac{(N - \bar{N}_{in})^2}{\sigma_{in}^2} \right) \right] \\ &+ C_{out} \left[\exp \left(-\frac{(N - N_{out})^2}{\sigma_{out}^2} \right) + \exp \left(-\frac{(N - \bar{N}_{out})^2}{\sigma_{out}^2} \right) \right], \end{aligned} \quad (3)$$

where V_0 is a constant parameter, N_{CN} is the neutron number of the compound nucleus, N_j ($j = in, out$) determines the (inner and outer) peak positions of heavy fragments taking care of shell effects, and \bar{N}_j ($\bar{N}_j \equiv N_{CN} - N_j$) determines those of light fragments. The factor $\exp(-\gamma\varepsilon(N))$ in Eq. (2) with the damping parameter γ is for the quenching of the shell effects at high excitation energies [30] with $\varepsilon(N) \equiv E^* - [V_{mac}(N) + V_{sh}(N)]$.

In the previous works [13,14], the emission of prompt neutrons were taken into account in the fission barrier $V(N)$ by using the average number of emitted neutrons $\bar{\nu}$ known for each compound nucleus. Therefore, the center of the fission yield distribution and the light fragment peaks were shifted by $\bar{\nu}$ through $\tilde{N}_{CN} \equiv N_{CN} - \bar{\nu}$ and $\tilde{N}_j \equiv \tilde{N}_{CN} - N_j$ ($j = in, out$), respectively. In other words, in Refs. [13,14], where Eq. (3) was applied to describe the POST-FPY, \tilde{N}_{CN} and \tilde{N}_j were used in Eq. (3) in place of N_{CN} and \bar{N}_j . Then, the model was applied to reproduce the POST-FPY data by using the unchanged charge density postulate

$$\frac{N}{A} = \frac{N_{CN} - \bar{\nu}}{A_{CN} - \bar{\nu}}, \quad (4)$$

which allows us to express our calculation results as a function of the fragment mass A instead of the fragment neutron number N through the average value $\bar{\nu}$ of the neutron multiplicity.

It is generally thought that the prompt neutrons are emitted from the nascent fission products. Primary fission product yields before emitting the prompt neutrons would have mirror symmetric shapes because the yields of heavy fragments and those of the counter-part light fragments are expected to be the same except for the rare cases of ternary fission. Thus, it is more appropriate to apply Eqs. (1)~(3), which would give us mirror symmetric yields, to

the *pre*-neutron emission FPY rather than the POST-FPY. Also, if the neutron multiplicity is available for each fission fragment mass, as can be obtained from the experimental data [31–38], we can treat the neutron multiplicity as a function of each fission fragment mass as $\nu = \nu(A^*)$. By doing so, we may attempt to describe both the PRE- and POST-FPYs in a consistent manner. Because we apply Eqs. (1)~(3) to the PRE-FPY, Eq. (4) needs to be changed to $N/A = N_{CN}/A_{CN}$ in converting the FPY from a function of N to that of A . Unfortunately, there are only a few PRE-FPY data available, while quite a few POST-FPY data exist. We also need the neutron multiplicity data $\nu(A^*)$ for each fragment mass. The systems where both PRE- and POST-FPY data are available together with the neutron multiplicity data $\nu(A^*)$ are just $^{233}\text{U}(n_{th},f)$, $^{235}\text{U}(n_{th},f)$ and $^{239}\text{Pu}(n_{th},f)$. Thus, we only consider these three systems in applying the model.

III. MODEL PARAMETERS TO REPRODUCE THE PRE-NEUTRON EMISSION FPY

As seen in Eqs. (1)~(3), our model has ten parameters in total: C_{mac} , C_{in} , C_{out} , V_0 , N_{in} , N_{out} , σ_{in} , σ_{out} , γ and \tilde{a} . C_{mac} determines the curvature of the macroscopic part of the fission barrier, $V_{mac}(N)$. We used Eqs. (8) and (9) of Ref. [39] for C_{mac} that was fixed from the width of fission fragment mass distribution at high excitation energies [40]. Since the Gaussian functions of $V_{sh}(N)$ in Eq. (3) take care of modulation of the fission barrier due to neutron shell effects, we fix the value of N_{in} as 82 to take into account the shell effect of spherical nuclei and treat N_{out} as an adjustable parameter. Although the fission barrier heights of different isotopes may vary, the same value of $V_0 = 5$ MeV may be used for all uranium and plutonium isotopes as in Refs. [13] and [14], respectively. From the earlier analysis of level density parameters of nuclides, the damping parameter γ was found to be $(0.05 \sim 0.06)$ MeV $^{-1}$ [41] which was consistent with the results ($\gamma = 0.05$ MeV $^{-1}$) of a microscopic shell model calculation [30]. We use the value of $\gamma = 0.06$ MeV $^{-1}$ by following Ref. [42].

Therefore, only six parameters (C_{in} , C_{out} , N_{out} , σ_{in} , σ_{out} and \tilde{a}) are left and they are determined by fitting the *pre*-neutron emission FPY data. As noted in Sect.II, in Refs. [13, 14] the model was initially applied to the *post*-neutron FPY data by using the average values of neutron multiplicity ($\bar{\nu}$) for each compound nucleus. However, in this work we apply

the model to the PRE-FPY data and calculate the POST-FPY by using the experimental neutron multiplicity $\nu(A^*)$ available for each fission fragment mass to be discussed in the next section. Nuclear data libraries such as the ENDF and JEFF provide recommended values only for the POST-FPY. The experimental data of the PRE-FPY [37,38,43–52] have been measured by using different methods, most of which are based on the 2E method. The 2E method requires the average number of neutrons as a function of the fragment masses in the analysis. The most accurate PRE-FPY experimental data available are those in Ref. [45] taken by the 2E-1V method for ^{233}U , ^{235}U , and ^{239}Pu , and those in Ref. [37] taken by the 2E-2V method for ^{239}Pu . Therefore, the PRE-FPY data in Refs. [37,45] are employed to find the model parameters. The six adjustable parameters are determined by minimizing $\langle\Delta Y^2\rangle$ defined by

$$\langle\Delta Y^2\rangle \equiv \frac{1}{i_{max}} \sum_{i=1}^{i_{max}} (Y_i - \bar{Y}_i)^2, \quad (5)$$

where i_{max} is the number of the data points, Y_i is the calculated yield, and \bar{Y}_i is the experimental yields from Refs. [37,45]. The resulting ten parameters of the model are summarized in Table 1. For comparison, the parameters obtained earlier by reproducing the POST-FPY for uranium [13] and plutonium [14] isotopes are also listed.

In Fig. 1, the six parameters fixed by the least square fit of the PRE-FPY for $^{233}\text{U}(n_{th},f)$, $^{235}\text{U}(n_{th},f)$ and $^{239}\text{Pu}(n_{th},f)$ are plotted together with those fixed in the previous works applied to the POST-FPY of uranium and plutonium isotopes. The model parameters obtained to reproduce the PRE-FPY data are in general similar to those [13,14] obtained to reproduce the POST-FPY except for $^{239}\text{Pu}(n_{th},f)$. The parameters of the present work for ^{233}U and ^{235}U are quite similar to those obtained for the POST-FPY of uranium isotopes. The PRE-FPYs calculated with the parameters in Table 1 are plotted by the black solid curves in the right panels of Fig. 2 together with those calculated by the GEF which also provides the pre-neutron fission product mass distribution. Because the GEF takes into account the even-odd effects in the proton and neutron number of fission fragments, there are spikes in the results of the GEF. All the experimental data as well as the data [37, 45] used in the analyses are plotted on the left panels. The experimental data for ^{233}U and ^{235}U of Ref. [45] are denoted by the red circles in the upper right and middle right panels. The average values of the experimental data for ^{239}Pu from Refs. [37,45] are plotted by the red circles in the lower right panel. The values of $\langle\Delta Y^2\rangle$ calculated from the GEF and

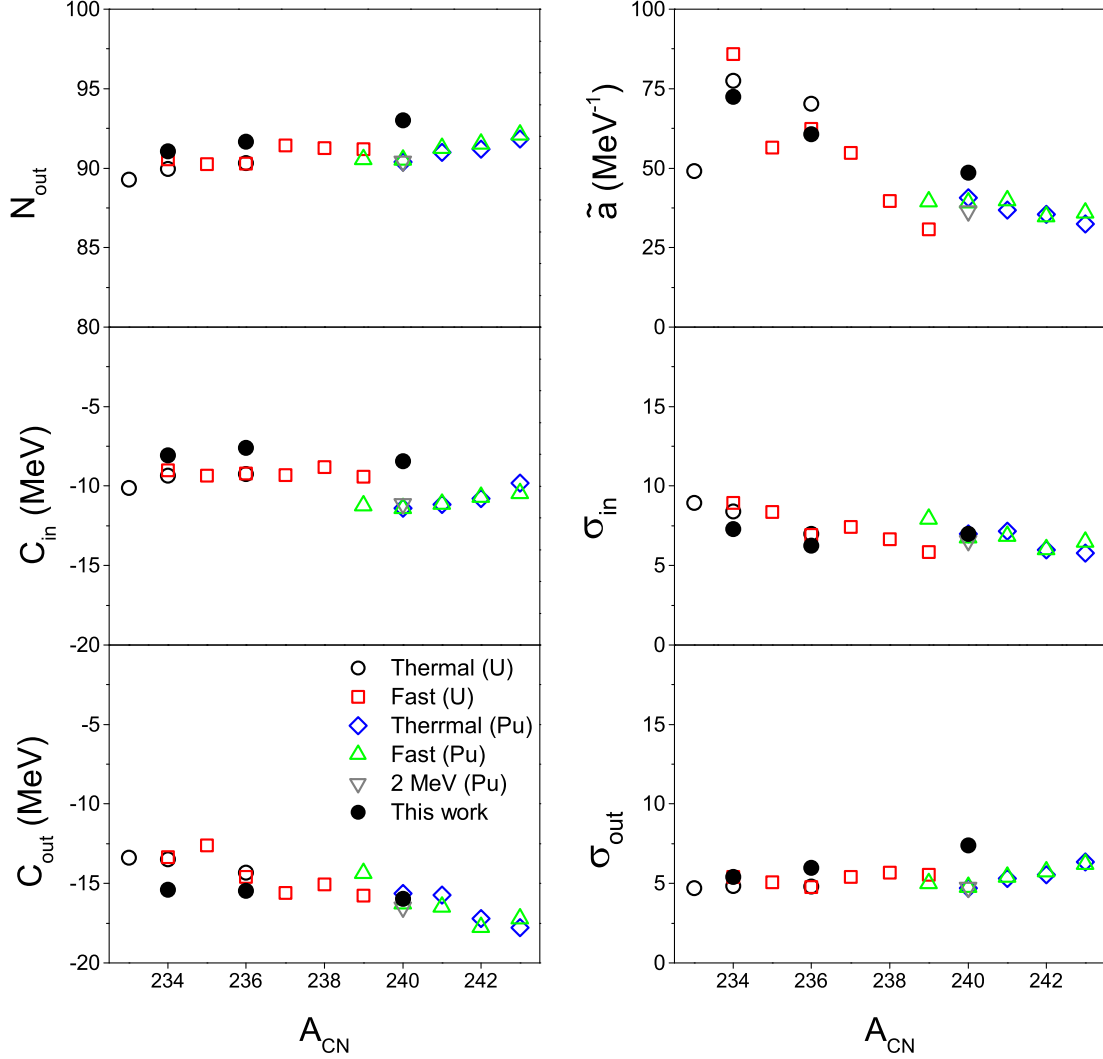


Fig. 1. The six parameters extracted to reproduce the *pre*-neutron FPY of thermal neutron-induced fission of ^{233}U , ^{235}U and ^{239}Pu are compared with those of the previous works [13,14] obtained to reproduce the *post*-neutron FPY data of uranium and plutonium isotopes. The black solid circles represent the parameters obtained in this work for uranium and plutonium isotopes. The various open symbols represent the parameters extracted in Refs. [13,14]. The black empty circles and red empty squares denote the parameters for reproducing the POST-FPY due to thermal and 500 keV neutron-induced fission of uranium isotopes, respectively. The blue rhombuses, green triangles and gray reversed triangles represent, respectively, those for thermal, 500 keV and 2 MeV neutron-induced fission of plutonium isotopes.

Table 1. The model parameters listed in the middle column are determined to reproduce the PRE-FPY of thermal neutron-induced fission of ^{233}U , ^{235}U and ^{239}Pu , and are compared with those obtained earlier [13,14] to reproduce the POST-FPY.

	^{233}U	^{235}U	^{239}Pu	U (post) [Ref. [13]]	Pu (post) [Ref. [14]]
N_{out}	91.36	93.02		90.50	91.08
C_{in} (MeV)	-7.83	-8.43		-9.31	-10.9
C_{out} (MeV)	-15.4	-16.0		-14.2	-16.5
\tilde{a} (MeV $^{-1}$)	72.5	60.7	48.6	11.6(241 - A_{CN})	2.50(256 - A_{CN})
σ_{in}	7.28	6.24	6.99	0.662(248 - A_{CN})	0.51(254 - A_{CN})
σ_{out}	5.40	5.97	7.39	5.13	5.38
V_0 (MeV)	5.0				
γ (MeV $^{-1}$)	0.06				
N_{in}	82				
C_{mac} (MeV)	Eqs. (8) and (9) of Ref. [39]				

Table 2. The values of $\langle\Delta Y^2\rangle$ for the PRE-FPY calculated by the GEF and our semi-empirical fission model

Fission	No. of data points	GEF	This work
$^{233}\text{U}(n_{th},f)$	87	0.205	0.055
$^{235}\text{U}(n_{th},f)$	83	0.134	0.049
$^{239}\text{Pu}(n_{th},f)$	95	0.073	0.006
Average		0.137	0.037

our model are listed in Table 2. Because our model parameters are fitted to reproduce the PRE-FPY data by minimizing $\langle\Delta Y^2\rangle$, the values of $\langle\Delta Y^2\rangle$ from our model are much smaller than those from the GEF.

IV. FROM PRE- TO POST-NEUTRON EMISSION FPY

Once the PRE-FPY is calculated, we can attempt to calculate the POST-FPY by using the neutron multiplicity data available for ^{233}U , ^{235}U , and ^{239}Pu . The neutron multiplic-

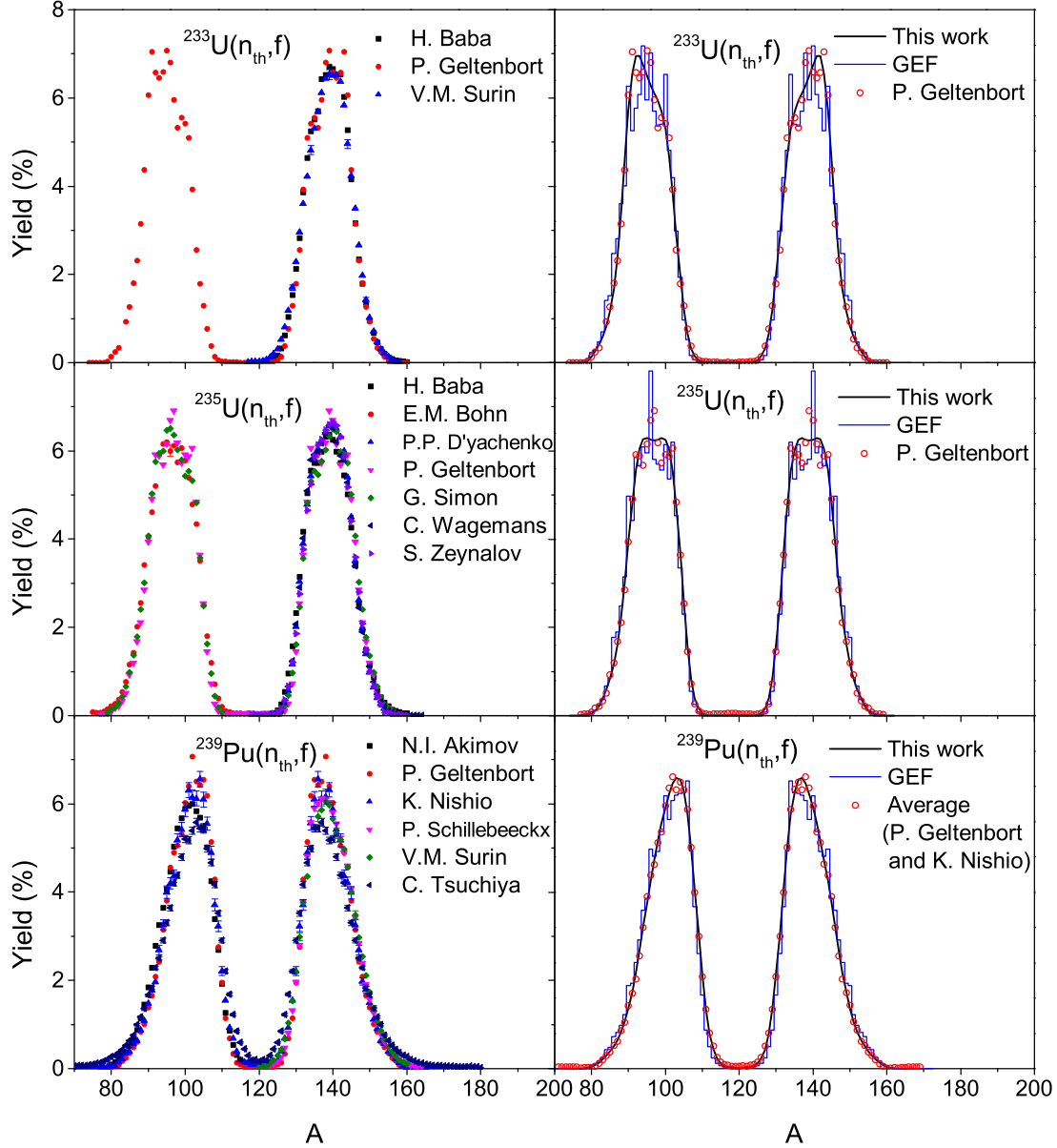


Fig. 2. Our calculation results for the PRE-FPY of ^{233}U , ^{235}U and ^{239}Pu by using the parameters in Table 1 are plotted on the right panels by the black full curves. The experimental data [37, 45] are denoted by the red circles on the right panels. The PRE-FPY obtained by the GEF is plotted by the blue histogram. All the experimental PRE-FPY data available from the EXFOR are plotted on the left panels for comparison.

ities measured by different experimental groups have discrepancies from each other. Not all the measured neutron multiplicity data in the EXFOR [53] have experimental uncertainties listed. Thus, we took the averages of the experimental neutron multiplicities for

each fragment mass without considering the uncertainties. The experimental values of neutron multiplicities with arbitrary units [54,55] or non-integer fragment masses [56] are not included in the calculation. Also, some experimental data sets have missing neutron multiplicities for certain fragment masses. Such data sets are not included in the calculation. Then, we are left with only one set of experimental neutron multiplicity data for $^{233}\text{U}(n_{th},f)$ [31], which is shown in the upper panel of Fig. 3. For $^{235}\text{U}(n_{th},f)$ and $^{239}\text{Pu}(n_{th},f)$, there are five [32–36] and three [32,37,38] sets of data, respectively. The experimental neutron multiplicities for ^{235}U and ^{239}Pu are averaged to get $\nu(A^*)^{avg}$ and are plotted in the middle and bottom panels of Fig. 3, respectively. Then, the POST-FPY Y_{post} may be deduced from the PRE-FPY Y_{pre} as follows.

Let $P_n(A^*)$ be the probability that a pre-neutron emission fragment with a mass number A^* decays to a post-neutron emission fragment with a mass number $A = A^* - n$ by the emission of n neutrons. Then, $Y_{post}(A)$ can be written as

$$Y_{post}(A) = \sum_n Y_{pre}(A+n)P_n(A+n), \quad (6)$$

where $n = 0, 1, 2, \dots$, and the measured neutron multiplicity of a pre-fragment with a mass number A^* , $\nu(A^*)$, would be given by

$$\nu(A^*) = \sum_n nP_n(A^*) \quad (7)$$

with the normalization condition

$$\sum_n P_n(A^*) = 1. \quad (8)$$

These relations are not sufficient to determine $P_n(A^*)$. In fact, there was an experimental work to extract $P_n(A^*)$ for spontaneous fission of Cf and Fm isotopes [57], where $P_n(A^*)$ seemed to have mostly Gaussian-shaped distributions while for some cases with small values of neutron multiplicity $P_n(A^*)$ seemed to have Poisson-shaped distributions. (Note that for Cf and Fm isotopes, $\bar{\nu}$ is relatively large as $3\sim 4$.) $P_n(A^*)$ extracted in Ref. [57] was not for each fission fragment mass number A^* but for small ranges of A^* . Also, it was extracted from each fission event with no distinction between light and heavy fragments. On the other hand, $P_n(A^*)$ in Eqs. (6)~(8) is for each fission fragment with a mass number A^* . Thus, we resort to the following three assumptions for $P_n(A^*)$.

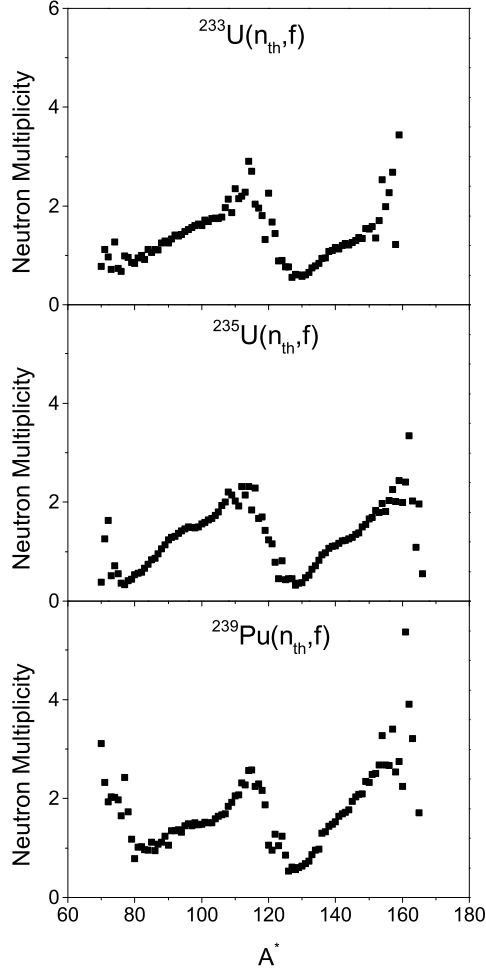


Fig. 3. The neutron multiplicities shown in the top panel for ^{233}U is from Ref. [31], while those in the middle (for ^{235}U) and the bottom (for ^{239}Pu) are the averaged values $\nu(A^*)^{avg}$. (See the text for details.) These neutron multiplicities are taken as $P_n(A^*)$ for the 2-point approximation and averaged Poisson distribution.

(1) 2-point distribution: $P_n(A^*)$ may be assumed to be determined by two consecutive integer values of n_1 and $n_1 + 1$ which are closest to the experimental neutron multiplicity values. In other words, we assume that

$$P_n^{2P}(A^*) = \begin{cases} 1 - r_1, & \text{for } n = n_1, \\ r_1, & \text{for } n = n_1 + 1, \\ 0, & \text{for other } n, \end{cases} \quad (9)$$

where n_1 and r_1 are, respectively, the integer and the fractional part of the averaged neutron multiplicity, $\nu(A^*)^{avg}$ shown in Fig. 3. That is, $n_1 \equiv \lfloor \nu(A^*)^{avg} \rfloor$ and $r_1 \equiv \nu(A^*)^{avg} - n_1$.

$[\nu(A^*)^{avg}]$, where $[x]$ denotes the greatest integer less than or equal to a real number x . We refer to this $P_n^{2P}(A^*)$ as the 2-point distribution.

(2) Averaged Poisson distribution: We may assume that $P_n(A^*)$ follows the Poisson distribution

$$P_n^{PS}(\lambda) = \frac{\lambda^n e^{-\lambda}}{n!} \quad (10)$$

with the parameter λ being the *average* value of $\nu(A^*)$. We take the average experimental neutron multiplicities shown in Fig. 3 for the value of λ . The values of $\nu(A^*)^{avg}$ for almost all fission fragments are less than 4, and thus we may assume that n , the number of emitted neutrons, can run up to 10 for practical calculations so that the cumulative Poisson distribution is larger than 0.99.

As an alternative to $P_n^{PS}(n; \lambda)$, we also considered the binomial distribution

$$P_n^{BI}(n_{max}, p) = \frac{n_{max}!}{n!(n_{max} - n)!} p^n (1 - p)^{n_{max} - n}, \quad (11)$$

where $n(= 0, 1, 2, \dots, n_{max})$ corresponds to the number of emitted neutrons with another parameter n_{max} and $p = \nu(A^*)^{avg}/n_{max}$. However, we find that Y_{post} calculated by using the binomial distribution P_n^{BI} is practically the same as that from P_n^{PS} . Therefore, the results by using the binomial distribution are not shown here.

(3) Optimized Poisson distribution: Another way of determining $P_n(A^*)$ is to use the Poisson distribution of Eq. (10), but instead of using $\lambda = \nu(A^*)^{avg}$ we look for the values of λ for each A^* to minimize the value χ_S^2 defined by

$$\begin{aligned} \chi_S^2 &= \chi_Y^2 + \chi_\nu^2 \\ &= \frac{1}{i_{max}} \sum_{i=1}^{i_{max}} \left(\frac{Y_i - Y_i^{exp}}{\Delta Y_i^{exp}} \right)^2 + \frac{1}{j_{max}} \sum_{j=1}^{j_{max}} \left(\frac{\nu_j - \nu_j^{exp}}{\Delta \nu_j^{exp}} \right)^2. \end{aligned} \quad (12)$$

In Eq. (12), i_{max} and j_{max} are the number of yield data and neutron multiplicity data, respectively, and Y_i and ν_j are the fission yield and neutron multiplicity calculated by Eqs. (6) and (7), respectively. Y_i^{exp} and ΔY_i^{exp} are the fission yield data and the uncertainties from the ENDF/B-VII.1, while ν_j^{exp} and $\Delta \nu_j^{exp}$ are the experimental neutron multiplicity data and their uncertainties shown in Fig. 4. In this third method, λ in Eq. (10) is treated as a free parameter determined by minimizing χ_S^2 for each fission fragment mass number A^* . The neutron multiplicities λ determined in this way are plotted in Fig. 4 by the black solid lines,

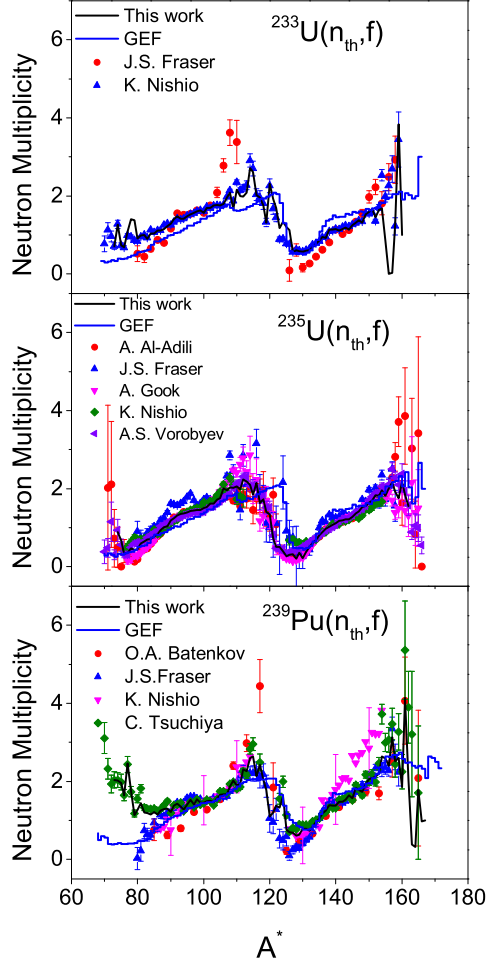


Fig. 4. The neutron multiplicities for $^{233}\text{U}(n_{th},f)$, $^{235}\text{U}(n_{th},f)$ and $^{239}\text{Pu}(n_{th},f)$ obtained by minimizing χ^2_{ξ} in Eq. (12) with the optimized Poisson distribution for $P_n(A)$ are plotted by the black solid curves in comparison with the experimental data used in the calculations. For comparison, the neutron multiplicities calculated by the GEF are presented by the blue step lines.

which agree in general with the experimental data. We denote such neutron multiplicity λ by $\nu(A^*)^{opt}$ to distinguish them from $\nu(A^*)^{avg}$.

$Y_{post}(A)$ s calculated in these three methods for $P_n(A^*)$ are compared with the experimental yield data and the ENDF evaluated data in Figs. 5 and 6. $Y_{post}(A)$ calculated for ^{233}U , ^{235}U and ^{239}Pu by using the 2-point distribution is presented in the right panels of Fig. 5 by the black step lines together with the ENDF/B-VII.1 [1] data plotted by the gray dots with error bars. For comparison, the results from the GEF 2021/1.1 model [26] are plotted on the left panels by the blue solid step lines. The experimental data [15–25] from the EXFOR library are denoted by different symbols as indicated in Fig. 5. $Y_{post}(A)$ calculated

by using the averaged Poisson distribution and the optimized Poisson distribution are presented by the solid step lines in the left and right panels of Fig. 6, respectively. Among the experimental data available in the EXFOR library, those data taken by using radiochemical separations [15,19], mass spectrometers [16,18,20–25], and catcher foil technique [17] are known to be more accurate than those measured by the 2E method. Thus, only the data from Ref. [15–25] are shown in Figs. 5 and 6.

Due to the mirror symmetric characteristics of smooth functions in Eqs. (1)~(3), the detailed fluctuating structures in the POST-FPY were not reproduced in Refs. [13,14]. On the other hand, by using $Y_{pre}(A^*)$ calculated by Eqs. (1)~(3) and taking into account the neutron multiplicities, not only the overall shapes of the POST-FPY but also some detailed structures near the peaks seem to be reproduced better than in Refs. [13,14]. The 2-point approximation seems very crude, but $Y_{post}(A)$ calculated by the 2-point approximation appears to reproduce the experimental POST-FPY data as seen in Fig. 5. The spike at $A = 134$ of $^{239}\text{Pu}(n_{th},f)$ seems reproduced by the 2-point approximation as seen in the lower right panel of Fig. 5. On the other hand, the Poisson distributions with smooth mass distributions result in $Y_{post}(A)$ with little fluctuating structures as seen in Fig. 6.

In Fig. 7, $P_n(A^*)$ from the 2-point distribution, averaged Poisson and optimized Poisson distributions for $^{239}\text{Pu}(n_{th},f)$ are plotted for $A^* = 135, 139$ and 159 by the black squares, the red circles, and the blue triangles, respectively. These choices are made because they correspond to the cases of $\nu(A^*) \approx 1, 1.5$ and 3 . When the value of $\nu(A^* = 135)^{avg} = 0.981$, very close to 1, P_n is concentrated at $n = 1$ in the 2-point distribution as can be seen in the upper panel of Fig. 7. As a result, most of the fission fragments with $A^* = 135$ contribute to the generation of the spike at $A = 134$ of the POST-FPY of ^{239}Pu in the 2-point distribution by emitting one neutron. (See the bottom right panel of Fig. 5.) On the other hand, the value of $P_n(A^* = 135)$ from the averaged and optimized Poisson distributions do not exceed 0.4 and have relatively broad distributions as shown in the top panel of Fig. 7, which cannot generate sharp fluctuation structures in the POST-FPY. As the value of $\nu(A^*)^{avg}$ increases, P_n s of both Poisson distributions become broader and the peak positions are shifted to the right as seen in the middle and lower panels of Fig. 7. When $\nu(A^* = 139)^{avg} = 1.48$, close to 1.5, P_n is evenly distributed in the 2-point approximation as seen in the middle panel of Fig. 7. When $\nu(A^* = 159)^{avg} = 2.75$, close to 3, the Poisson distributions are further shifted to the right and become similar to a Gaussian distribution, as it should.

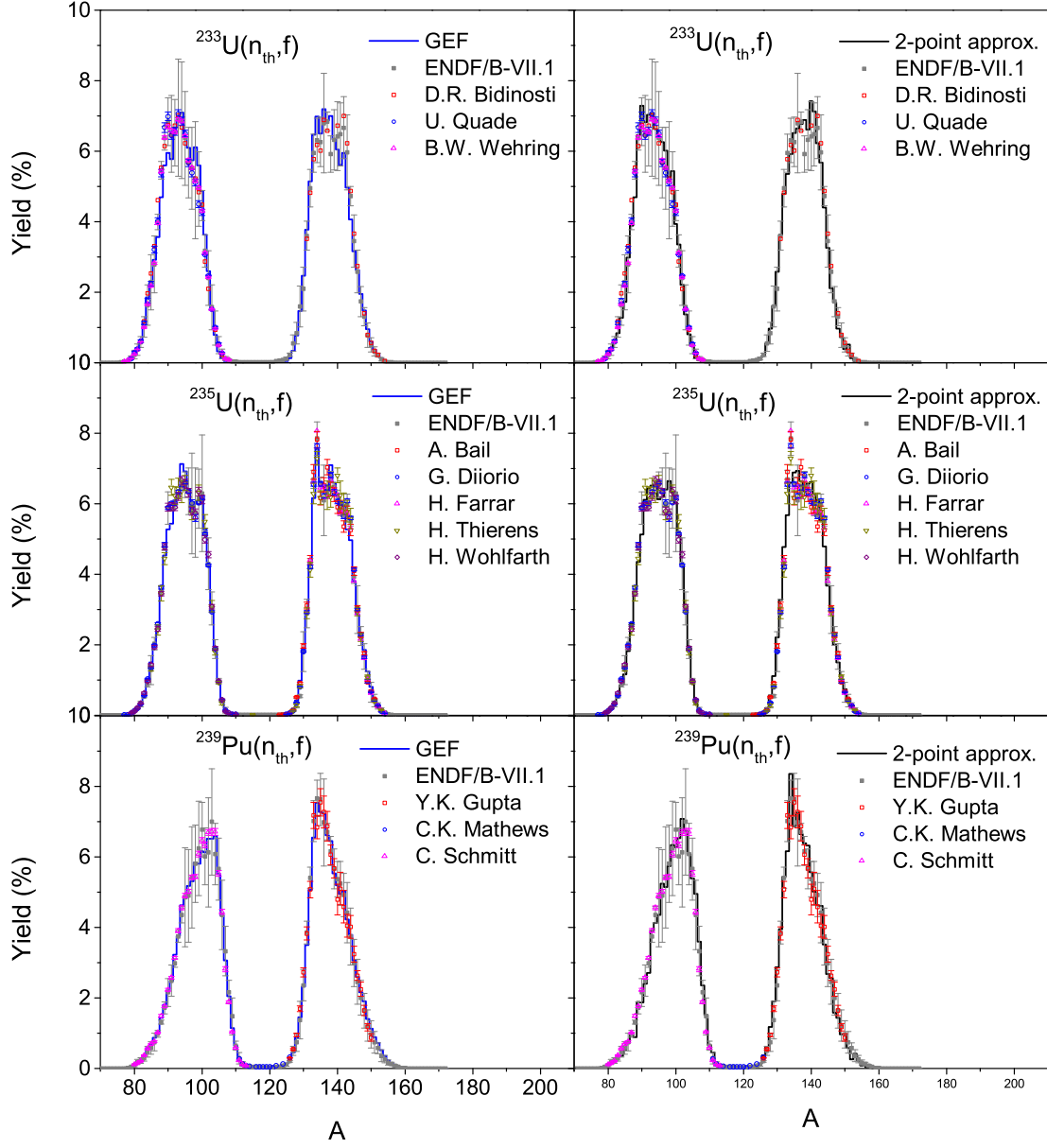


Fig. 5. The POST-FPY for the thermal neutron-induced fission of ^{233}U , ^{235}U and ^{239}Pu are plotted. $Y_{post}(A)$ calculated by using the 2-point approximation (the black step lines) is compared with the GEF (the blue step lines) and the ENDF/B-VII.1 data (the gray dots with error bars). Experimental data [15–25] from the EXFOR library are represented by different symbols.

We remark that the spike at $A = 134$ in the ENDF data for ^{235}U is not reproduced by the 2-point approximation as seen in the middle right panel of Fig. 5 though a similar spike at $A = 134$ is reproduced for ^{239}Pu . This is due to the use of the averaged value of neutron multiplicity $\nu(A^*)^{avg}$. If we use the experimental neutron multiplicity data of

Fraser [32], where $\nu(135)$ is 0.997, close to 1, then the spike at $A = 134$ is again well reproduced. Our results of the POST-FPY shown in Figs. 5 and 6 seem to suggest that the 2-point approximation, being a naive, simple model, seems useful in reproducing the spike particularly when $\nu(A^*)$ is close to 1. As $\nu(A^*)$ becomes larger, $P_n(A^*)$ seems to follow close to a Poisson distribution as Fig. 7 shows. If $\nu(A^*)$ becomes even larger, $P_n(A^*)$ seems to follow a Gaussian distribution, as Ref. [57] shows.

To see quantitatively the degree of agreement between the calculation results and the ENDF data, we list in Table 3 the values of χ_Y^2 of Eq. (12) and those of $\langle \Delta Y^2 \rangle$ calculated by using the ENDF data as the experimental POST-FPY. Though our model parameters were fitted to reproduce the PRE-FPY data rather than the post-neutron data, the values of $\langle \Delta Y^2 \rangle$ calculated for the POST-FPY from our model are similar to those from the GEF. On the other hand, the values of χ_Y^2 from our model are somewhat larger than those from the GEF. Note that the GEF is a sophisticated model with about 50 parameters while our model has essentially six adjustable parameters. In the case of ^{235}U , the uncertainties in the FPY data are small for all the fragments because of a large amount of accumulated experimental data. Therefore, the values of χ_Y^2 for ^{235}U are larger than those for ^{233}U and ^{239}Pu in both our model and the GEF. Note that the values of χ_Y^2 from the optimized Poisson distribution are a little smaller than those from the averaged Poisson distribution while the two Poisson distributions look quite similar to each other as seen in Fig. 7. Out of nearly 90 data points of A^* , there are just about 5 data points for each isotope where the two Poisson distributions do not agree well, though they are not shown here. Those few points are all in the valley or in the wing regions, where the evaluated uncertainties of yields are very small. Due to the small uncertainties of yields, the values of χ_Y^2 from the two Poisson distributions are different, though $P_n(A^*)$ s look very similar for most values of A^* .

At present, there are not many cases where PRE- and POST-FPY and neutron multiplicity data are available simultaneously. There is no recommended value like the ENDF data for the PRE-FPY. The neutron multiplicity values from different experimental groups have discrepancies. Thus, more experimental FPY and neutron multiplicity data are needed to describe the PRE- and POST-FPY in a consistent way.

V. SUMMARY

Table 3. $\langle\Delta Y^2\rangle$ and χ_Y^2 values calculated by the GEF and our model for the POST-FPY

Fission	No. of data points	$\langle\Delta Y^2\rangle$				χ_Y^2			
		GEF	2-point approx.	Avg. Poisson	Opt. Poisson	GEF	2-point approx.	Avg. Poisson	Opt. Poisson
$^{233}\text{U}(n_{th},f)$	85	0.1217	0.0848	0.0532	0.0337	1.17	1.92	1.40	1.02
$^{235}\text{U}(n_{th},f)$	86	0.0361	0.0970	0.0911	0.0831	4.09	6.68	7.63	5.52
$^{239}\text{Pu}(n_{th},f)$	88	0.0335	0.0786	0.0534	0.0562	0.40	2.08	1.13	1.24
Average		0.0638	0.0868	0.0659	0.0576	1.89	3.56	3.39	2.60

We applied a semi-empirical model to compute first the PRE-FPY of thermal neutron-induced fission of ^{233}U , ^{235}U and ^{239}Pu , and then calculated the POST-FPY by using the neutron multiplicity data. In our previous works [13, 14], the semi-empirical model was applied to the POST-FPY taken from the “ENDF/B-VII.1”. In this work, however, the model parameters were fixed to reproduce the experimental PRE-FPY data. The six model parameters obtained to reproduce the PRE-FPY were in general close to those obtained to reproduce the POST-FPY except for ^{239}Pu . The POST-FPY are then calculated by using the model parameters fixed to the primary FPY and the neutron multiplicity data with three different assumptions about the probability of the number of emitted neutrons for each fission fragment mass number A^* : 2-point approximation, averaged Poisson distribution and optimized Poisson distribution. The resulting POST-FPYs obtained from the three different assumptions reproduce the overall shapes of the POST-FPY from the ENDF. Although the 2-point distribution is a very simple and naive assumption, it shows a possibility to describe the fluctuating structures of the POST-FPY. In particular, when $\nu(A^*)$ is less than ~ 1.5 , $P_n(A^*)$ may be well approximated to the 2-point distribution. As $\nu(A^*)$ increases, $P_n(A^*)$ seems to follow the Poisson distribution. If $\nu(A^*)$ further increases, $P_n(A^*)$ seems to follow the Gaussian distribution. Though the model parameters were determined to reproduce the pre-neutron data, the values of $\langle\Delta Y^2\rangle$ and χ_Y^2 , indicating the degree of agreement between the calculated POST-FPY and the ENDF data, are comparable to those of the GEF. If more accurate neutron multiplicity data are available, we can test the model better.

ACKNOWLEDGMENTS

This work was supported in part by the National Research Foundation (NRF) of Korea funded by the Ministry of Science and ICT (NRF-2020R1A2C1102384, NRF-2018M7A1A1072274). TSP acknowledges the support from the IBS grant funded by the Korean government (No. IBS-R031-D1).

REFERENCES

- [1] M. Chadwick et al., Nucl. Data Sheets **112**, 2887 (2011).
- [2] A.J.M. Plompen et al., Eur. Phys. J. A **56**, 181 (2020).
- [3] H. Goutte, J.F. Berger, P. Casoli, D. Gogny, Phys. Rev. C **71**, 024316 (2005).
- [4] G. Scamps, C. Simenel, D. Lacroix, Phys. Rev. C **92**, 011602 (2015).
- [5] D. Regnier, N. Dubray, N. Schunck, M. Verrière, Phys. Rev. C **93**, 054611 (2016).
- [6] J. Zhao, J. Xiang, Z.-P. Li, T. Nikšić, D. Vretenar, S.-G. Zhou, Phys. Rev. C **99**, 054613 (2019).
- [7] A.V. Karpov, P.N. Nadtochy, D.V. Vanin, G.D. Adeev, Phys. Rev. C **63**, 054610 (2001).
- [8] T. Asano, T. Wada, M. Ohta, T. Ichikawa, S. Yamaji, H. Nakahara, J. Nucl. Radiochem. Sci. **5**, 1 (2004).
- [9] J. Randrup, P. Möller, A.J. Sierk, Phys. Rev. C **84**, 034613 (2011).
- [10] Y. Aritomo, S. Chiba, Phys. Rev. C **88**, 044614 (2013).
- [11] K. Mazurek, C. Schmitt, P.N. Nadtochy, Phys. Rev. C **91**, 041603 (2015).
- [12] S. Okumura, T. Kawano, P. Jaffke, P. Talou, S. Chiba, J. Nucl. Sci. Technol. **55**, 1009 (2018).
- [13] J. Lee, C.-S. Gil, Y.-O. Lee, T.-S. Park, S.W. Hong, Eur. Phys. J. A **54**, 173 (2018).
- [14] J. Lee, Y.-O. Lee, T.-S. Park, S.W. Hong, J. Korean Phys. Soc. **77**, 1082 (2020).
- [15] D.R. Bidinosti, D.E. Irish, R.H. Tomlinson, Can. J. Chem. **39**, 628 (1961).
- [16] H. Farrar, R.H. Tomlinson, Nucl. Phys. **34**, 367 (1962).
- [17] H. Thierens, D. de Frenne, E. Jacobs, A. de Clercq, P. D'Hondt, A.J. Deruytter, Nucl. Instrum. Methods **134**, 299 (1976).
- [18] G. Diiorio, B.W. Wehring, Nucl. Instrum. Methods **147**, 487 (1977).
- [19] C.K. Mathews, Phys. Rev. C **15**, 344 (1977).
- [20] H. Wohlfarth, PhD Thesis, Technische Hochschule Darmstadt (1977).

- [21] B.W. Wehring, S. Lee, G. Swift, *Light fragment independent yields for thermal neutron fission of U-233*, UILU-ENG-80-5312, University of Illinois, Urbana (1980).
- [22] C. Schmitt et al., Nucl. Phys. A **430**, 21 (1984).
- [23] U. Quade et al., Nucl. Phys. A **487**, 1 (1988).
- [24] A. Bail, PhD Thesis, University of Bordeaux (2009).
- [25] Y.K. Gupta et al., Phys. Rev. C **96**, 014608 (2017).
- [26] K.-H. Schmidt, B. Jurado, C. Amouroux, C. Schmitt, Nucl. Data Sheets **131**, 107 (2016).
- [27] N. Bohr, J.A. Wheeler, Phys. Rev. **56**, 426 (1939).
- [28] P. Fong, Phys. Rev. **102**, 434 (1956).
- [29] K.-H. Schmidt, A. Kelić, M.V. Ricciardi, Europhys. Lett. **83**, 23001 (2008).
- [30] A.V. Ignatyuk, G.N. Smirenkin, A.S. Tishin, Sov. J. Nucl. Phys. **21**, 255 (1975).
- [31] K. Nishio, M. Nakashima, I. Kimura, Y. Nakagome, J. Nucl. Sci. Technol.(Tokyo) **35**, 631 (1998).
- [32] J.S. Fraser, J.C.D. Milton, Ann. Rev. Nucl. Sci. **16**, 379 (1966).
- [33] K. Nishio, Y. Nakagome, H. Yamamoto, I. Kimura, Nucl. Phys. A **632**, 540 (1998).
- [34] A.S. Vorobyev, O.A. Shcherbakov, A.M. Gagarski, G.V. Val'ski, G.A. Petrov, EPJ Web Conf. **8**, 03004 (2010).
- [35] A. Göök, F.-J. Hamsch, S. Oberstedt, M. Vidali, Phys. Rev. C **98**, 044615 (2018).
- [36] A. Al-Adili, D. Tarrío, K. Jansson, V. Rakopoulos, A. Solders, S. Pomp, A. Göök, F.-J.Hamsch, S. Oberstedt, M. Vidali, Phys. Rev. C **102**, 064610 (2020).
- [37] K. Nishio, Y. Nakagome, I. Kanno, I. Kimura, J. Nucl. Sci. Technol.(Tokyo) **32**, 404 (1995).
- [38] C. Tsuchiya, Y. Nakagome, H. Yamana, H. Moriyama, K. Nishio, I. Kanno, K. Shin, I. Kimura, J. Nucl. Sci. Technol.(Tokyo) **37**, 941 (2000).
- [39] J. Benlliure, A. Grewe, M. de Jong, K.-H. Schmidt, S. Zhdanov, Nucl. Phys. A **628**, 458 (1998).
- [40] M.G. Itkis, V.N. Okolovich, A.Ya. Rusanov, G.N. Smirenkin, Sov. J. Part. Nucl. **19**, 301 (1988).
- [41] A. S. Iljinov et al., Nucl. Phys. A **543**, 517 (1992).
- [42] T. von Egidy, D. Bucurescu, Phys. Rev. C **72**, 044311 (2005).
- [43] P. Schillebeeckx, C. Wagemans, A.J. Deruytter, R. Barthélémy, Nucl. Phys. A **545**, 623 (1992).
- [44] V.M. Surin, A.I. Sergachev, N.I. Rezchikov, B.D. Kuzminov, Sov. J. Nucl. Phys. **14**, 523

- (1972).
- [45] P. Geltenbort, F. Gönnerwein, A. Oed, *Radiat. Effects* **93**, 57 (1986).
 - [46] H. Baba et al., *J. Nucl. Sci. Technol. (Tokyo)* **34**, 871 (1997).
 - [47] E.M. Bohn, B.W. Wehring, M.E. Wyman, *Phys. Rev.* **188**, 1909 (1969).
 - [48] P.P. D'yachenko, B.D. Kuz'minov, M.Z. Tarasko, *Sov. J. Nucl. Phys.* **8**, 165 (1969).
 - [49] G. Simon, J. Trochon, F. Brisard, C. Signarbieux, *Nucl. Instrum. Methods Phys. Res. A* **286**, 220 (1990).
 - [50] C. Wagemans, L. Demattè, S. Pommé, P. Schillebeeckx, *Nucl. Phys. A* **597**, 188 (1996).
 - [51] S. Zeynalov et al., Investigation of mass-TKE distribution of fission fragments from the $^{235}\text{U}(n,f)$ -reaction in resonances, *Conf: International Seminar on Interactions of Neutrons with Nuclei*, No.13, p.351 (2006).
 - [52] N.I. Akimov et al., *Sov. J. Nucl. Phys.* **13**, 272 (1971).
 - [53] V.V. Zerkin, B.Pritychenko, *Nucl. Instrum. Methods Phys.Res. A* **888**, 31 (2018).
 - [54] V.A. Korostylev, D.K.Ryazanov, V.A.Safonov, *Proceedings of the Conference on Neutron Physics* Vol.2, p.78 (1971).
 - [55] Y.S. Zamyatnin, B.G. Basova, D.K. Ryazanov, A.D. Rabinovich, V.A. Korostylev, *Sov. J. Nucl. Phys.* **27**, 31 (1978).
 - [56] V.F. Apalin, Yu.N. Gritsyuk, I.E. Kutikov, V.I. Lebedev, L.A. Mikaelian, *Nucl. Phys.* **71**, 553 (1965).
 - [57] D.C. Hoffman, G.P. Ford, J.P. Balagna, L.R. Veaser, *Phys. Rev. C* **21**, 637 (1980).

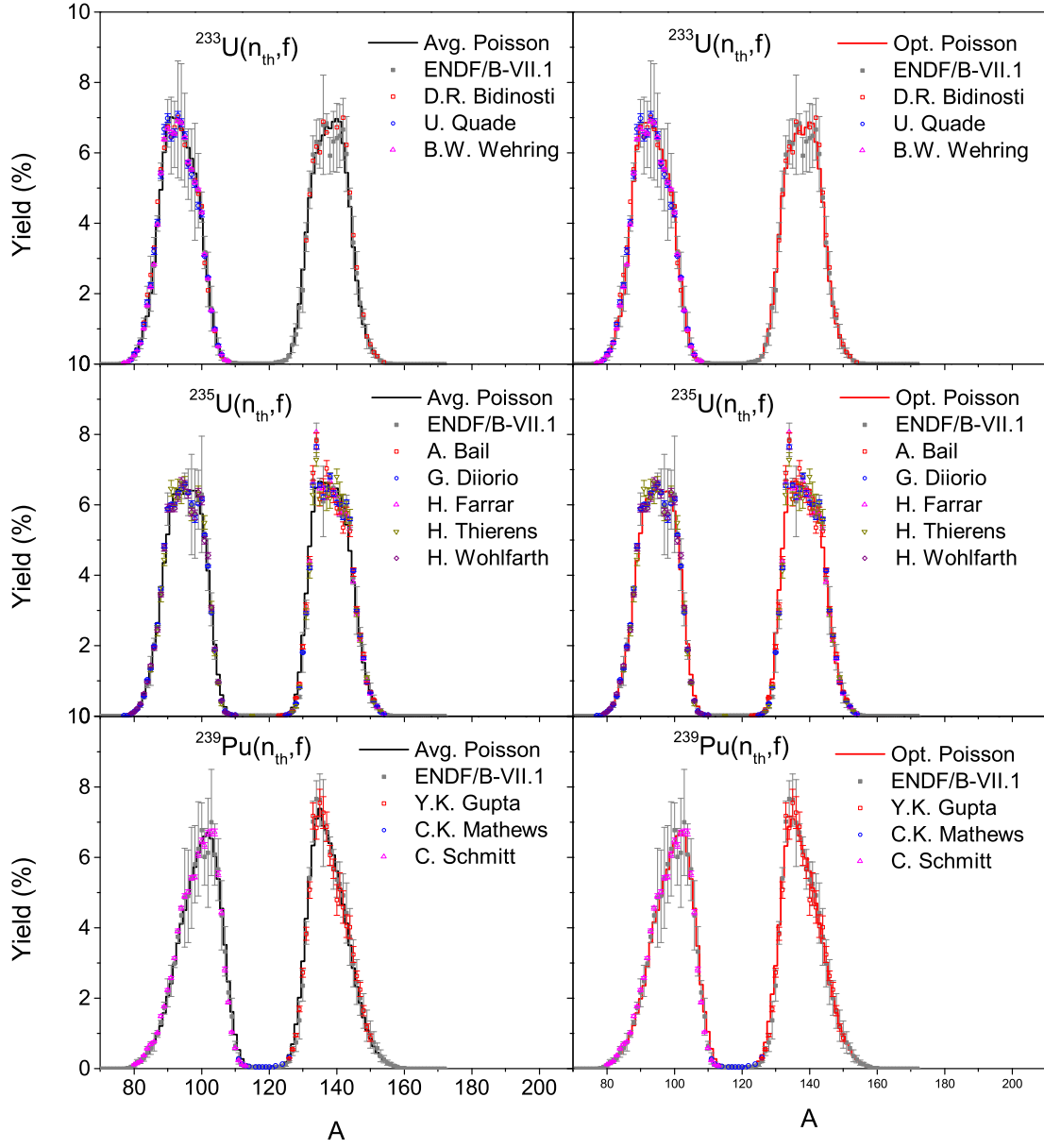


Fig. 6. The POST-FPY for the thermal neutron-induced fission of ^{233}U , ^{235}U and ^{239}Pu are plotted. $Y_{post}(A)$ calculated by using the averaged Poisson distribution (the black step lines) are plotted on the left panels in comparison with the ENDF/B-VII.1 data (the gray dots with error bars). Y_{post} calculated by using the optimized Poisson distribution are plotted by the red step lines on the right panels.

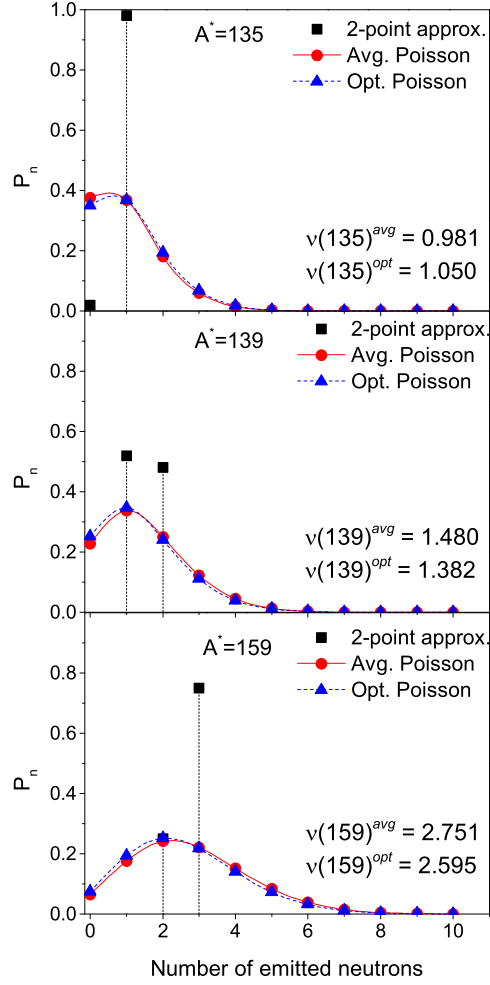


Fig. 7. $P_n(A^*)$ distributions are plotted for the 2-point distribution, averaged Poisson and optimized Poisson distribution for the cases of $^{239}\text{Pu}(n_{th},f)$ with $A^* = 135$ (upper panel), $A^* = 139$ (middle panel) and $A^* = 159$ (lower panel) by the black squares, the red circles, and the blue triangles, respectively. $\nu(A^*)^{avg}$ and $\nu(A^*)^{opt}$ refer to the average value of the experimental neutron multiplicity data shown in Fig. 3 and the neutron multiplicity obtained by minimizing the value of χ_s^2 of Eq. (12), respectively.